

The Importance of Nonlinear Cross-Shelf Momentum Flux during Wind-Driven Coastal Upwelling*

STEVEN J. LENTZ AND DAVID C. CHAPMAN

Woods Hole Oceanographic Institution, Woods Hole, Massachusetts

(Manuscript received 18 April 2003, in final form 25 May 2004)

ABSTRACT

A simple theory is proposed for steady, two-dimensional, wind-driven coastal upwelling that relates the dynamics and the structure of the cross-shelf circulation to the stratification, bathymetry, and wind stress. The new element is an estimate of the nonlinear cross-shelf momentum flux divergence due to the wind-driven cross-shelf circulation acting on the vertically sheared geostrophic alongshelf flow. The theory predicts that the magnitude of the cross-shelf momentum flux divergence relative to the wind stress depends on the Burger number $S = \alpha N/f$, where α is the bottom slope, N is the buoyancy frequency, and f is the Coriolis parameter. For $S \ll 1$ (weak stratification), the cross-shelf momentum flux divergence is small, the bottom stress balances the wind stress, and the onshore return flow is primarily in the bottom boundary layer. For $S \approx 1$ or larger (strong stratification), the cross-shelf momentum flux divergence balances the wind stress, the bottom stress is small, and the onshore return flow is in the interior. Estimates of the cross-shelf momentum flux divergence using moored observations from four coastal upwelling regions ($0.2 \leq S \leq 1.5$) are substantial relative to the wind stress when $S \approx 1$ and exhibit a dependence on S that is consistent with the theory. Two-dimensional numerical model results indicate that the cross-shelf momentum flux divergence can be substantial for the time-dependent response and that the onshore return flow shifts from the bottom boundary layer for small S to just below the surface boundary layer for $S \approx 1.5$ –2.

1. Introduction

Wind-driven coastal upwelling typically brings cold, nutrient-rich subsurface waters to the surface, fueling phytoplankton growth. As a result, coastal upwelling regions, such as the west coasts of North and South America, are some of the most biologically productive areas in the world oceans and the sites of some of the world's largest fisheries (Barber and Smith 1981). This has motivated a substantial effort over the last three decades to study coastal upwelling regions and more generally the wind-driven circulation (see the following review articles: Winant 1980; Allen 1980; Huyer 1990; Smith 1995; Brink 1998; Strub et al. 1998; Hickey 1998; Badan-Dangon 1998; Shillington 1998). While significant progress has been made in understanding some aspects of coastal upwelling (e.g., the alongshelf flow), many features of the cross-shelf and vertical circulation remain poorly understood (e.g., Lentz 1995; Brink 1998).

Mean current profiles from midshelf sites in several coastal upwelling regions illustrate some of the limitations of our understanding of the cross-shelf circulation (Fig. 1). The mean wind stresses are upwelling favorable at these sites and the cross-shelf velocity profiles during individual upwelling-favorable wind events are similar to the mean profiles (see, e.g., Fig. 3 in Smith 1981). The mean cross-shelf velocity profiles are qualitatively consistent with two-dimensional coastal upwelling in the sense that there is an offshore flow in the upper 20–30 m of the water column, and an onshore return flow below this surface layer. The offshore and onshore transports are not equal, as would be the case if the flow were strictly two-dimensional (i.e., no alongshelf variations), but there is a tendency for the two transports to balance. However, there are substantial differences in the vertical structure of the onshore return flow at these four sites. The onshore mean flow over the northwest Africa shelf (Fig. 1a) is in the lower half of the water column with the maximum onshore flow near the bottom. On the northern California shelf (Fig. 1b), the onshore flow is weak with a maximum at about middepth, 50 m in 90 m of water. On the Oregon shelf (Fig. 1c), the onshore flow is concentrated just below the surface boundary layer (20–60-m depth), with the maximum onshore flow at about 40 m in 103 m of water. Over the Peru shelf (Fig. 1d), the onshore flow spans

* Woods Hole Oceanographic Institution Contribution Number 10934.

Corresponding author address: Dr. Steven J. Lentz, MS 21, Woods Hole Oceanographic Institution, Woods Hole, MA 02543.
E-mail: slentz@whoi.edu

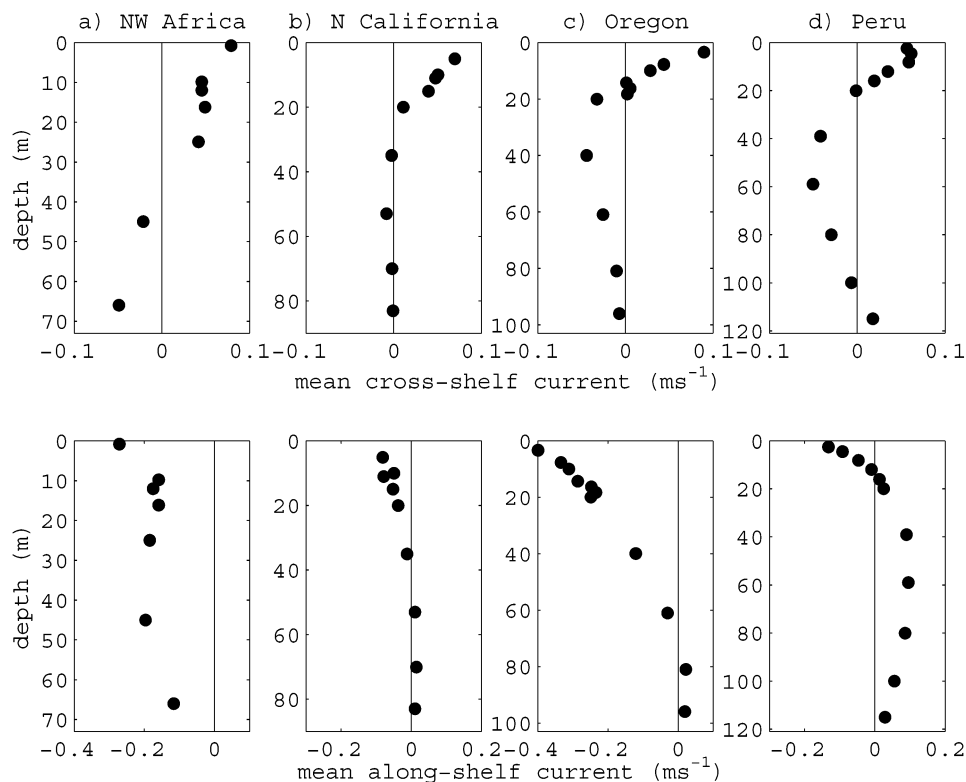


FIG. 1. (top) Mean cross-shelf and (bottom) alongshelf current profiles from four midshelf mooring sites (after Smith 1981). Burger number S increases from (a) to (d) (see Table 1). Positive currents are offshore and poleward alongshelf. Northern California profiles are for 1982, and the Peru profiles are from mooring PS. Note depth scales are different for each site.

most of the water column below the surface boundary layer, with the maximum onshore flow at middepth and the hint of an offshore flow near the bottom. At present, it remains unclear what determines the observed vertical structure of the cross-shelf velocity and the variations in the structure for different coastal upwelling regions. Yet, the vertical structure of the cross-shelf velocity and the associated vertical velocity are critical to understanding the consequences of upwelling, such as the redistribution of nutrients. For example, an onshore return flow in the upper half of the water column, as off Oregon, may be less effective at bringing nutrients into the euphotic zone than a deeper onshore return flow, as off northwest Africa.

The structure of the cross-shelf velocity is closely tied to the alongshelf momentum balance. However, despite numerous observational studies (Scott and Csanady 1976; Allen and Kundu 1978; Allen and Smith 1981; Hickey 1984; Lee et al. 1984, 1989; Lentz and Winant 1986; Lentz et al. 1999), the depth-averaged alongshelf momentum balance over most shelves remains unclear because of uncertainties in bottom stress estimates, difficulties in accurately measuring alongshelf pressure gradients, and uncertainties in the Coriolis force associated with the often small depth-averaged cross-shelf velocities. In the steady depth-integrated alongshelf mo-

mentum balance, the wind stress could be balanced by an alongshelf pressure gradient, the Coriolis force associated with the cross-shelf transport, bottom stress, or the divergence in nonlinear advection of momentum. Only the latter two are a possibility for purely two-dimensional flow (no alongshelf variations). If bottom stress balances the wind stress, then the return flow is concentrated in the bottom boundary layer, and its magnitude is determined by the alongshelf velocity at the bottom (Ekman 1905). Of the examples in Fig. 1, only northwest Africa is consistent with this balance. Early observations by Sverdrup (1938) of interior onshore flow during upwelling off California motivated a number of theoretical studies attributing the interior onshore flow to an alongshelf pressure gradient (e.g., Garvine 1971). Subsequently, alongshelf pressure gradients were shown to be a substantial component of the subtidal alongshelf momentum balance on many shelves (e.g., Allen and Smith 1981; Lentz and Winant 1986). However, as noted by Smith (1981), direct evidence linking alongshelf pressure gradients to the vertical structure of the onshore flow does not exist. In numerical modeling studies, an alongshelf pressure gradient opposing the wind stress reduces the cross-shelf flow within the bottom boundary layer, but there is no substantial improvement in reproducing the observed cross-shelf velocity

profiles (Zamudio and López 1994; Federiuk and Allen 1995). The contribution of nonlinear advection of momentum in the depth-averaged momentum balance has rarely been estimated or considered in theory [though see Pedlosky (1978) for an exception], although both observations (Allen and Kundu 1978) and numerical modeling results (Federiuk and Allen 1995) suggest that nonlinear advection of momentum may be substantial over the Oregon shelf.

To examine both the alongshelf momentum balance and the cross-shelf circulation during wind-driven coastal upwelling, a steady two-dimensional theory is proposed that relates the depth-integrated dynamics to the characteristics of the stratification and bathymetry (section 2). (Henceforth two-dimensional implies no alongshelf variations in the flow. An imposed alongshelf pressure gradient is included in the theory.) The new element is the inclusion and estimation of the nonlinear cross-shelf momentum flux divergence in the alongshelf momentum balance. This is not a complete theory for two-dimensional coastal upwelling because it does not address the evolution of the density field. Instead, the density structure is defined a priori using scaling arguments. Nevertheless, this two-dimensional model, though clearly an oversimplification, allows us to isolate the role of the nonlinear cross-shelf momentum flux and provides a clearer understanding of the underlying physics that can be applied to observations and more realistic numerical studies. Furthermore, previous numerical modeling studies (e.g., Federiuk and Allen 1995) and observational studies of the heat balance (Bryden et al. 1980; Richman and Badan-Dangon 1983; Lentz 1987; Dever and Lentz 1994) indicate that a two-dimensional perspective is relevant to many coastal upwelling regions.

The key result of this study is the demonstration that different shelf stratifications and bathymetries can produce variations in the magnitude of the nonlinear cross-shelf momentum flux divergence and, hence, in the vertical structure of the wind-driven cross-shelf flow, even in the absence of alongshelf variations (i.e., no alongshelf pressure gradient). For completeness and comparison to observations, the theory is extended to include an alongshelf pressure gradient (section 2c). Analysis of existing observations from several coastal upwelling regions supports this prediction and shows that the cross-shelf momentum flux divergence is substantial relative to the wind stress in some coastal upwelling regions (section 3). The importance of the nonlinear cross-shelf momentum flux divergence during the spin-up of an upwelling circulation is demonstrated using a two-dimensional, primitive equation, numerical model (section 4).

2. Theory

Consider a two-dimensional, wind-driven, stratified flow over a sloping bottom (Fig. 2). Assuming there are

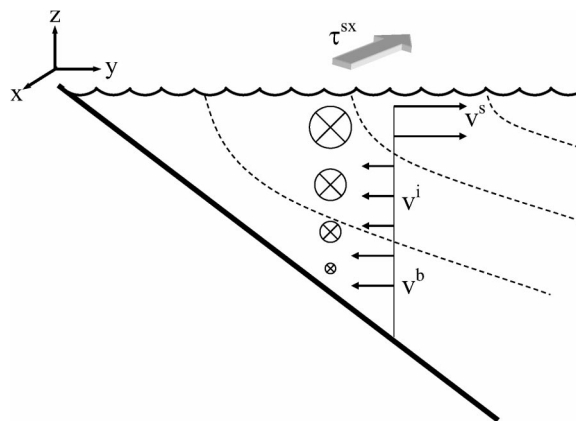


FIG. 2. Schematic of the assumed structure of the cross-shelf flow and isopycnals in response to an upwelling-favorable wind stress. There is a wind-driven offshore flow in the surface boundary layer v^s and onshore flows in the interior v^i and bottom boundary layer v^b , such that the offshore transport balances the onshore transport. The geostrophic alongshelf flow is in the direction of the wind stress and decreases linearly with depth.

no alongshelf variations in the flow ($\partial \mathbf{u} / \partial x = 0$) and sea level variations are small in comparison with the water depth, continuity requires that

$$\int_{-h}^0 v \, dz = 0 \quad (1)$$

everywhere since there can be no cross-shelf transport at the coast ($y = 0$). Here h is the water depth, v is the cross-shelf component of flow, and y and z are the cross-shelf and vertical coordinates, respectively. The depth-integrated alongshelf momentum balance, using (1), is

$$\frac{\partial}{\partial t} \int_{-h}^0 u \, dz + \frac{\partial}{\partial y} \int_{-h}^0 uv \, dz = -gh \frac{\partial \eta}{\partial x} + \frac{\tau^{sx}}{\rho_o} - \frac{\tau^{bx}}{\rho_o}, \quad (2)$$

where u is the alongshelf velocity; $\partial \eta / \partial x$ is an imposed alongshelf sea level gradient, τ^{sx} and τ^{bx} are the alongshelf components of the surface and bottom stress, respectively, ρ_o is a reference density, and g is gravitational acceleration. The barotropic alongshelf pressure gradient is included for completeness. Thus, for two-dimensional flow, temporal changes in the alongshelf transport are caused by the divergence in the cross-shelf momentum flux, an alongshelf pressure gradient, the wind stress, and the bottom stress.

Scaling arguments and observations (e.g., Brown et al. 1987) indicate that the cross-shelf momentum balance is primarily geostrophic over most shelves—that is, a balance between the cross-shelf pressure gradient and Coriolis force associated with the alongshelf flow. Furthermore, there is substantial observational evidence indicating that the vertical shear in the alongshelf flow (Fig. 1, lower panels) is in thermal wind balance with the cross-shelf density gradient (Huyer et al. 1979; Brink

et al. 1980; Winant et al. 1987; Lentz and Trowbridge 2001).

The thermal-wind shear in the alongshelf flow provides the potential for a nonlinear cross-shelf momentum flux during upwelling (or downwelling). For example, during upwelling, the faster near-surface alongshelf flow is carried offshore while the slower subsurface alongshelf flow is carried onshore (Fig. 2), resulting in a net offshore momentum flux. This is similar to the net offshore flux of heat during upwelling owing to warmer near-surface water being carried offshore while cooler subsurface waters are carried onshore. The theory proposed below for the momentum balance is analogous to the simple model for the wind-driven offshore heat flux during upwelling proposed by Lentz (1987). There must be a divergence in the cross-shelf momentum flux, assuming it is nonzero somewhere offshore, because the flux is zero at the coast. The goal here is to determine under what circumstances, if any, this contribution to the cross-shelf momentum flux divergence is substantial relative to the wind stress. Determining the cross-shelf momentum flux divergence requires estimates of the alongshelf and cross-shelf velocity profiles.

a. Estimation of the nonlinear cross-shelf momentum flux

An estimate of the alongshelf velocity profile is obtained by integrating the thermal wind balance vertically from the surface to a depth z , yielding

$$u(z) \approx u^s + \frac{g}{f\rho_o} \frac{\partial \rho}{\partial y} z, \quad (3)$$

where u^s is the velocity at the surface, f is the Coriolis parameter, and for simplicity the cross-shelf density gradient $\partial \rho / \partial y$ is assumed to be independent of z .

The cross-shelf velocity profile is assumed to consist of three components: wind-driven Ekman transport in a surface boundary layer of thickness δ^s , bottom-stress-driven Ekman transport in a bottom boundary layer of thickness δ^b , and an interior flow (as in Dever 1997). The vertically uniform, cross-shelf velocities are

$$v^s = -\frac{\tau^{sx}}{\rho_o f \delta^s}, \quad -\delta^s < z < 0, \quad (4)$$

$$v^i = \frac{\tau^{sx} - \tau^{bx}}{\rho_o f h}, \quad -h < z < 0, \quad \text{and} \quad (5)$$

$$v^b = \frac{\tau^{bx}}{\rho_o f \delta^b}, \quad -h < z < -h + \delta^b. \quad (6)$$

The interior velocity v^i in (5) follows from (1), (4), and (6).

There is substantial observational evidence from coastal upwelling regions supporting the assumption that the transport in the surface boundary layer nearly equals the wind-driven Ekman transport (Smith 1981;

Badan-Dangon et al. 1986; Winant et al. 1987; Lentz 1992) and that there is often a tendency for the onshore transport ($v^i h + v^b \delta^b$) to balance the offshore surface boundary layer transport (e.g., Smith 1981; Dever 1997; Lentz and Trowbridge 2001). The observational support for an Ekman balance in the bottom boundary layer is less substantial (Trowbridge and Lentz 1998; Lentz and Trowbridge 2001), due in part to the lack of near-bottom current and stress observations in coastal upwelling regions. The expectation that the interior cross-shelf flow v^i is vertically uniform, while convenient, is not supported by observations (e.g., Fig. 1). The assumption here is that the vertical structure of the flow affects the quantitative, but not the qualitative, results, and this is discussed in section 3b.

Given the vertical structure of $v(z)$ from (4)–(6) and $u(z)$ from (3), it is straightforward to integrate the product to estimate the nonlinear cross-shelf momentum flux (again making the assumption that $\partial \rho / \partial y$ is independent of z),

$$\int_{-h}^0 uv \, dz \approx \frac{g}{2\rho_o f} \frac{\partial \rho}{\partial y} \left[\frac{\tau^{sx}}{\rho_o f} (\delta^s - h) + \frac{\tau^{bx}}{\rho_o f} (\delta^b - h) \right]. \quad (7)$$

This estimate assumes contributions to the cross-shelf momentum flux, associated with the stress-driven vertical shears in the boundary layers, that would be present even in the absence of stratification, are relatively small. The numerical model calculations support this assumption for the time-dependent upwelling response (see section 3b).

The cross-shelf gradient of (7), assuming no cross-shelf variations in δ^s , δ^b , τ^{sx} , τ^{bx} , and $\partial \rho / \partial y$, is

$$\frac{\partial}{\partial y} \int_{-h}^0 uv \, dz \approx \frac{\tau^{sx}}{\rho_o f} \frac{\alpha N^2}{2f} \frac{\partial \rho / \partial y}{\partial \rho / \partial z} \left(1 + \frac{\tau^{bx}}{\tau^{sx}} \right), \quad (8)$$

where $\alpha = \partial h / \partial y$ is the bottom slope and $N^2 = -(g/\rho_o)(\partial \rho / \partial z)$ is the buoyancy frequency. Thus, in this model, the divergence in the cross-shelf momentum flux only occurs over a sloping bottom and where there are sloping isopycnals, that is, where there is thermal wind shear in the alongshelf flow. There would be no cross-shelf momentum flux far offshore where the isopycnals are level.

Previous theoretical studies indicate that the natural cross-shelf scale for the region of sloping isopycnals during upwelling is the baroclinic Rossby radius of deformation Nh/f (Charney 1955; Allen 1980). This suggests that the isopycnal slope should be proportional to the local water depth h divided by the local baroclinic deformation radius; that is,

$$\frac{\partial z}{\partial y} \Big|_{\rho} = -\frac{\partial \rho / \partial y}{\partial \rho / \partial z} \approx \pm a \frac{h}{(Nh/f)} = \pm a \frac{f}{N}, \quad (9)$$

where the sign is the same as the sign of the alongshelf wind stress, negative for upwelling, and a is a proportionality constant. For the upwelling regions in Fig. 1,

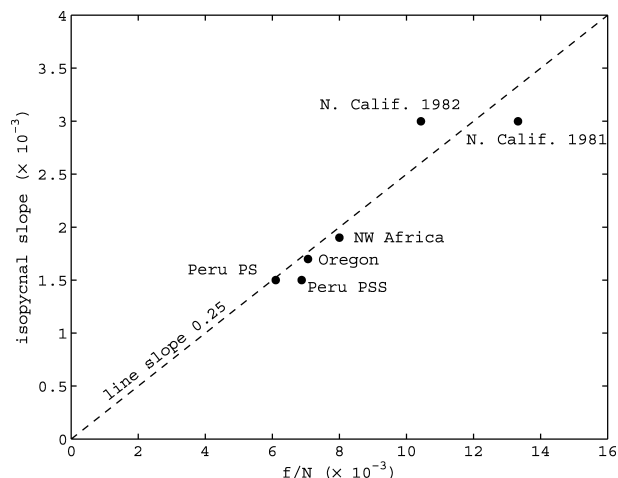


FIG. 3. Average isopycnal slopes as a function of f/N for each of the mooring sites. Isopycnal slopes were estimated from mean density sections shown in Brink et al. (1981) for Peru; Huyer and Smith (1985) for Oregon; Barton et al. (1977) for northwest Africa; Huyer (1984) for northern California 1981; and Huyer and Kosro (1987) for northern California 1982. The mean isopycnal slope for northwest Africa is uncertain because the slope is steeper over the outer half of the shelf than over the inner half of the shelf. The estimated isopycnal slope for Peru is representative of the upper 50 m of the water column because isopycnals slope down toward the coast below about 70-m depth.

mean isopycnals (from averaged density sections) slope upward toward the coast with a slope of about $0.25f/N$, supporting (9) with $a = 0.25$ (Fig. 3). Interestingly, the time-dependent numerical model results discussed in section 3b also yield isopycnal slopes of about $0.25f/N$ in the vicinity of the upwelling jet.

Using (9) to estimate the isopycnal slope, (8) may be written as

$$\frac{\partial}{\partial y} \int_{-h}^0 uv \, dz \approx -b \frac{|\tau^{sx}| S}{\rho_o} \left(1 + \frac{\tau^{bx}}{\tau^{sx}} \right), \quad (10)$$

where $S = \alpha N/f$ is the Burger number and the absolute value arises from the product of the wind stress and the isopycnal slope (both negative for upwelling). The proportionality constant b accounts for both the constant a in (9) and deviations from the assumed vertical structures of the cross-shelf and alongshelf velocity profiles (see Fig. 1). The estimate of the divergence in the cross-shelf momentum flux given by (10) depends only on the assumed velocity profiles (3)–(6). It does not depend on the size of the alongshelf pressure gradient, or whether or not the flow is steady. To proceed beyond (10) requires knowing how the bottom stress depends on τ^{sx} and S , which can be determined from the alongshelf momentum balance (2) as discussed next.

b. Steady, two-dimensional upwelling with no alongshelf pressure gradient

To gain insight into how the cross-shelf momentum flux divergence influences the dynamics and the cir-

ulation, consider first the simplest case: steady-state, no alongshelf pressure gradient, and an upwelling-favorable wind stress. Inclusion of an alongshelf pressure gradient is considered in section 2c, and the downwelling response ($\tau^{sx} > 0$) is discussed in section 4b. For this case, substituting (10) into (2) yields

$$\tau^{bx} \approx \tau^{sx} \frac{1 - bS/2}{1 + bS/2}. \quad (11)$$

Substitution of (11) into (10) provides a steady-state estimate of the divergence in the cross-shelf momentum flux during upwelling-favorable winds (assuming no alongshelf pressure gradient)

$$\frac{\partial}{\partial y} \int_{-h}^0 uv \, dz \approx \frac{\tau^{sx}}{\rho_o} \frac{bS}{1 + bS/2}. \quad (12)$$

In this case, both the bottom stress and the divergence in the cross-shelf momentum flux depend only on the Burger number and the alongshelf wind stress. As noted above, there is a cross-shelf momentum flux because the faster, near-surface alongshelf flow is carried offshore by the wind-driven Ekman transport in the surface boundary layer and is replaced by an onshore transport of the slower alongshelf flow in either the interior or the bottom boundary layer. There is a divergence in the cross-shelf momentum flux because the top-to-bottom alongshelf velocity difference increases as the water depth increases since the thermal wind shear is assumed constant. Consequently, the difference between the alongshelf velocity being carried offshore near the surface and the alongshelf velocity being returned onshore in the interior or near the bottom increases as the water depth increases. In (12), $(\tau^{sx}/\rho_o)S$ is the cross-shelf Ekman transport, $\tau^{sx}/(\rho_o f)$, multiplied by αN , which, using (3) and (9), can be shown to equal the cross-shelf gradient in the top-to-bottom alongshelf velocity difference due to changes in water depth. The factor $b/(1 + bS/2)$ accounts for the degree to which the onshore return flow is in the bottom boundary layer (S small) or in the interior (S order 1 or larger). This alters the cross-shelf momentum flux divergence because the top-to-interior alongshelf velocity difference is smaller than the top-to-bottom difference.

The theoretical dependence of the steady two-dimensional wind-driven upwelling response on S is evident from (11) and (12). Given the assumptions made in deriving (12), the divergence in the cross-shelf momentum flux is always negative during upwelling, so it will tend to balance (oppose) the wind stress. (In the following discussion b is assumed to be approximately 1 for simplicity). For small S , the divergence in the cross-shelf momentum flux is small from (12) (Fig. 4b line), and there is a balance between the surface stress and the bottom stress from (11) (Fig. 4a line). As a consequence, the onshore return flow is concentrated in the bottom boundary layer; that is, from (4)–(6) $v^b \delta^b \approx v^s \delta^s$ and $v_i h$ is small (Fig. 5 lines). As S increases,

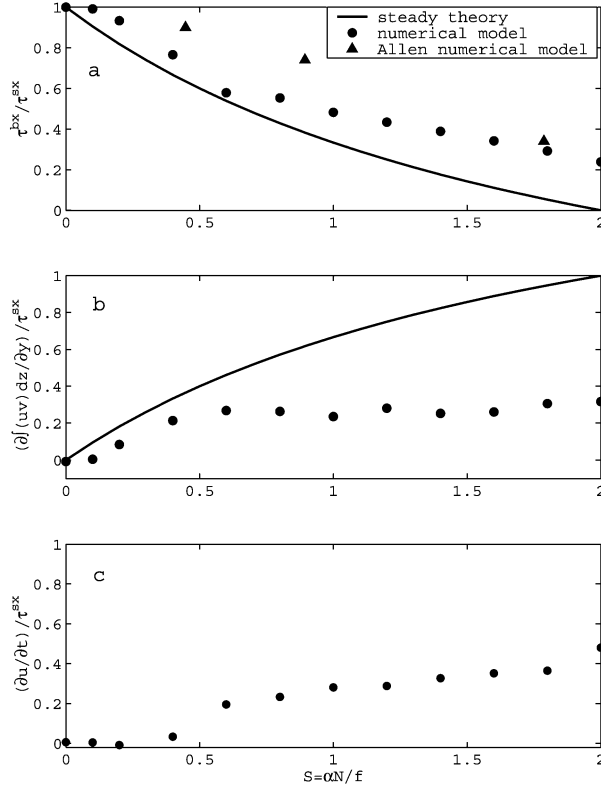


FIG. 4. Estimates of the terms in the vertically integrated alongshelf momentum balance, normalized by the wind stress, from the steady theory (lines, discussed in section 2b; $b = 1$) and the numerical model runs (●, discussed in section 3b). The normalized terms are (a) the bottom stress, (b) the divergence in the cross-shelf momentum flux, and (c) the temporal acceleration. Numerical model values are averages from day 12 to day 14 over the region between $y = 10$ km and $y = 20$ km. Results from three numerical model runs from Allen et al. (1995) are also shown (triangles) in (a).

the divergence in the cross-shelf momentum flux increases, the bottom stress decreases (Fig. 4), and there is a corresponding increase in v^i and decrease in v^b ; that is, more of the return flow occurs in the interior (Fig. 5). At $S = 2b^{-1}$ ($S = 2$ in Figs. 4 and 5), the bottom stress vanishes because the interior thermal wind shear is large enough to bring the near-bottom alongshelf flow to zero. Therefore, the wind stress is balanced by the cross-shelf momentum flux divergence, and all the return flow is in the interior. For $S > 2b^{-1}$, the theory suggests there is a reversal in the alongshelf flow near the bottom, so the bottom stress acts in the same direction as the wind stress, and both are balanced by the offshore momentum flux (not shown). However, in this case there would be offshore flow in the bottom boundary layer that would presumably cause the isopycnals to tilt in the opposite direction near the bottom, which is inconsistent with our assumption that the isopycnal slope is constant with depth. This emphasizes the major limitation of this model; a constant isopycnal slope given by (9) is assumed, rather than solving for the structure of the density field.

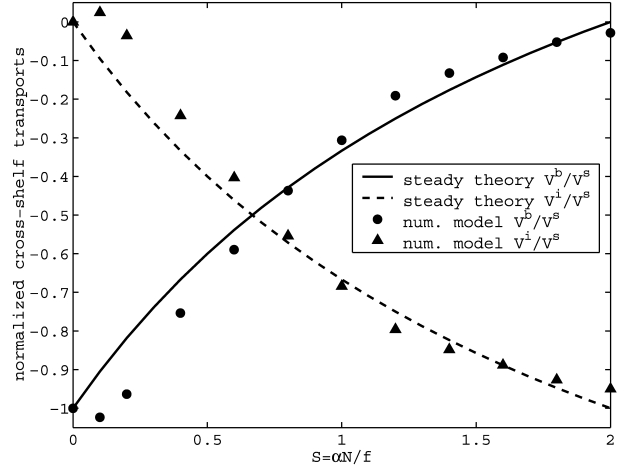


FIG. 5. The normalized cross-shelf transports in the interior (V^i/V^s) and the bottom boundary layer (V^b/V^s) as a function of the Burger number (S), from the steady theory (lines, discussed in section 2b) and the numerical model (symbols, discussed in section 3b). Numerical model values are after 13 days from a location 20 km offshore. Theoretical transports are calculated from (4)–(6) using (11) to estimate the bottom stress.

c. Steady, two-dimensional upwelling with an alongshelf pressure gradient

As noted above, observational studies of the alongshelf momentum balance in coastal upwelling regions have shown that alongshelf pressure gradients are often an important component of the subtidal dynamics (Allen and Smith 1981; Hickey 1984; Brown et al. 1987; Lentz 1994). Including the barotropic alongshelf pressure gradient in (2) for the case of steady, two-dimensional upwelling ($\tau^{sx} < 0$) and following the derivation in the previous section, the resulting estimates of the divergence in the cross-shelf momentum flux and the bottom stress are

$$\frac{\partial}{\partial y} \int_{-h}^0 uv dz \approx \left(\frac{\tau^{sx}}{\rho_o} - \frac{gh}{2} \frac{\partial \eta}{\partial x} \right) \frac{bS}{1 + bS/2} \quad \text{and} \quad (13)$$

$$\frac{\tau^{bx}}{\rho_o} \approx \frac{\tau^{sx}}{\rho_o} \left(\frac{1 - bS/2}{1 + bS/2} \right) - gh \frac{\partial \eta}{\partial x} \left(\frac{1}{1 + bS/2} \right). \quad (14)$$

The addition of a barotropic alongshelf pressure gradient in (13) modifies the forcing, but it does not change the dependence of the cross-shelf momentum flux divergence on S relative to (12). In contrast, the addition of a barotropic alongshelf pressure gradient in (14) does change the dependence of the bottom stress on S relative to (11). It will be shown in the following section that the bottom stress is often small (see also Allen and Smith 1981). In the case where the bottom stress is zero (considered in section 3a), from (13) and (14)

$$\frac{\partial}{\partial y} \int_{-h}^0 uv dz \approx \frac{\tau^{sx}}{\rho_o} \frac{bS}{2}. \quad (15)$$

TABLE 1. Parameters for each mooring site: β is the slope of the assumed linear relationship between temperature and density variations, α is the bottom slope, N is the buoyancy frequency, f is the Coriolis frequency, and $S = \alpha N/f$ is the Burger number; NC represents northern California.

Site	β $10^{-4} \text{ } ^\circ\text{C}^{-1}$	α 10^{-3}	N 10^{-3} s^{-1}	f 10^{-4} s^{-1}	S
Peru PSS	2.3	10	5.5	-0.38	1.50
Peru PS	2.3	7.5	6.2	-0.38	1.20
Oregon	3.5	6.7	14.6	1.03	0.95
NC 1982	3.5	5	8.7	0.91	0.48
NC 1981	3.5	5	6.8	0.91	0.38
NW Africa	1.5	1.5	6.7	0.54	0.19

From (14), the wind stress does not balance the along-shelf pressure gradient unless $S = 0$ (no stratification or no bottom slope) because of the contribution from the cross-shelf momentum flux divergence.

3. The importance of the cross-shelf momentum flux divergence

a. Observations

The proposed dependence of the cross-shelf momentum flux divergence on the wind stress and Burger number is tested using current observations from six mid-shelf mooring sites in coastal upwelling regions off Oregon (1973 CUE-2, site B), northwest Africa (1974 Joint 1, site Lisa), two Peru sites (1977 Joint 2, sites PS and PSS), and northern California in 1981 (CODE-1, site C3) and in 1982 (CODE-2, site C3) (Table 1). These sites were chosen because there are buoy wind observations and current observations spanning the water column at each site. Cross-shelf and alongshelf orientations are chosen based on the coastline orientation used in previous studies of the observations from each site (Lentz 1992). To estimate the Burger number S , the bottom slope α is determined from bathymetry sections (Smith 1981; Winant et al. 1987) and the Coriolis parameter f from the latitude (Table 1). The average buoyancy frequency N is estimated from the mean near-surface to near-bottom temperature difference assuming a linear relationship between temperature and density (Lentz 1992). The estimates of N are similar to estimates from the average density sections cited in section 2a because temperature is a reasonable proxy for density in these upwelling regions. The four upwelling sites span a relatively wide range of Burger numbers from 0.2 (NW Africa) to 1.5 (Peru) (Table 1).

The wind stress is estimated from the wind velocity and the anemometer heights following Large and Pond (1981). To be consistent with the two-dimensional theory, the depth-averaged cross-shelf flow is removed from v to obtain v' (Dever 1997). The vertical integral of uv' is then estimated using the hourly (unfiltered) currents and a trapezoidal rule, assuming no vertical variations in extrapolating to the surface and bottom. The cross-shelf divergence in the cross-shelf momentum

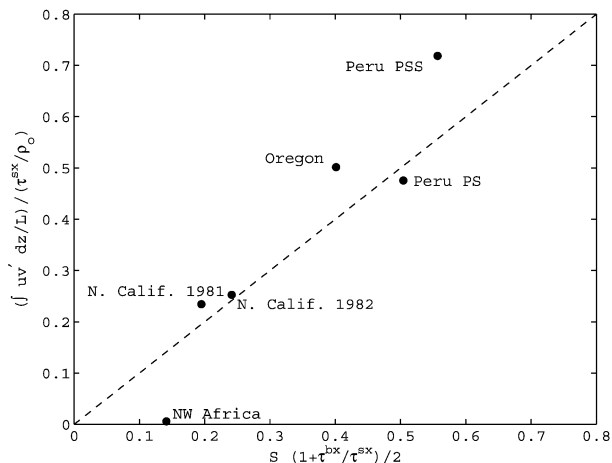


FIG. 6. Estimates of the ratio of the mean of $\int_{-h}^0 (uv') dz/L$ to the mean of (τ^{sx}/ρ_0) as functions of $S(1 + \tau^{bx}/\tau^{sx})/2$, the prediction given by (10), using observations from four coastal upwelling regions; L is distance to the coast.

flux is then estimated as the vertical integral of uv' divided by the distance to the coast (L), where the cross-shelf momentum flux must be zero. This is equivalent to integrating (12) from the coast to the mooring site and assuming there is no cross-shelf variation in the wind stress or Burger number. The resulting time series estimated using the unfiltered hourly data were then low-passed filtered (half-power point 33 h) to focus on the subtidal variability.

Direct estimates of the cross-shelf momentum flux divergence are first compared to estimates of the right-hand side of (8) because this estimates does not depend on either the alongshelf pressure gradient or the assumption of steady flow. Bottom stresses are estimated using a quadratic drag law

$$\tau^{bx} = C_d u_b (u_b^2 + v_b^2)^{1/2},$$

where (u_b, v_b) is the velocity measurement closest to the bottom and $C_d = 2.5 \times 10^{-3}$ (Lentz and Trowbridge 1991). The bottom stress estimates may not be accurate because of the uncertainty in C_d and the height of the near-bottom current observations (5–9 m). However, the comparison is not very sensitive to the bottom stress estimates because the ratio of τ^{bx}/τ^{sx} is small, 0.3 or less, except for northwest Africa where it is 0.8.

The mean divergence in the cross-shelf momentum flux is a significant fraction of the mean alongshelf wind stress for Peru and Oregon (ratios 0.5–0.75), but is small relative to the mean alongshelf wind stress for northwest Africa (Fig. 6). Thus, the nonlinear momentum flux terms are significant in some coastal upwelling regions, as previously suggested for Oregon by Allen and Kundu (1978). The agreement between the estimated mean cross-shelf momentum flux divergence and $S(1 + \tau^{bx}/\tau^{sx})/2$ supports the assumption that the cross-shelf momentum flux is due to the cross-shelf circulation acting on the thermal wind shear of the alongshelf flow and

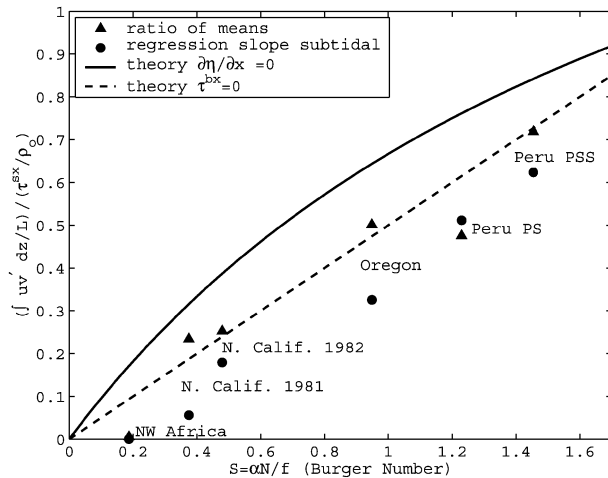


FIG. 7. The Burger number (S) dependence of estimates of the mean cross-shelf momentum flux divergence ($\int_0^L (uv') dz/L$) normalized by the wind stress (τ^{xy}/ρ_0) (triangles) and the linear regression slope of the subtidal cross-shelf momentum flux divergence vs the alongshelf wind stress (circles) using observations from four coastal upwelling regions; L is distance to the coast. The corresponding theoretical predictions from (13) for $\partial\eta/\partial x = 0$ (solid line) and for $\tau^{bx} = 0$ (dashed line) are also shown.

suggests the proportionality constant b is about 1. Direct estimates (not shown) indicate that most of the mean cross-shelf momentum flux ($\sim 75\%$) at each site is due to the mean cross-shelf circulation acting on the mean alongshelf velocity shear, that is the product of the mean profiles in Fig. 1. The exception is northern California in 1982 where the mean profiles only account for about 35% of the cross-shelf momentum flux divergence, possibly because of the contribution from mesoscale eddies (see below).

The ratio of the observed mean cross-shelf momentum flux divergence to the mean alongshelf wind stress is a nearly linear function of S with a slope of about 0.5 (Fig. 7, Table 2). The regression slope between the subtidal cross-shelf momentum flux divergence and the alongshelf wind stress is also roughly a linear function of S with a slope of about 0.5. Assuming that the flow is two-dimensional and the temporal acceleration term

is small (quasi-steady flow), (13) and (14) provide estimates of both the cross-shelf momentum flux divergence and the bottom stress in terms of the wind stress, alongshelf pressure gradient, and S (N , α , and f). Direct estimates of the mean alongshelf pressure gradient are not available, and so estimates were made assuming two extremes in (13), either that there is no alongshelf pressure gradient ($\partial\eta/\partial x = 0$, solid line Fig. 7) or that the bottom stress is zero, so that the wind stress is opposed by the alongshelf pressure gradient and the cross-shelf momentum flux divergence (dashed line Fig. 7). These two possibilities yield similar dependences on S . The observations are in better agreement with the latter, consistent with the bottom stress being small relative to the wind stress.

The observed divergence in the cross-shelf momentum flux is also related to the wind stress, in a manner consistent with the theory (Fig. 8). Off Peru and Oregon, where $S \approx 1$, the cross-shelf momentum flux divergence is substantial in comparison with the wind stress, and the two time series are correlated (Figs. 8a,b and Table 2). Off northern California and northwest Africa, where $S < 0.5$, the cross-shelf momentum flux divergence is generally small in comparison with the wind stress and is uncorrelated with the alongshelf wind stress (Figs. 8c,d). Off northern California there are also cross-shelf momentum flux events that are not obviously related to the wind stress. For example, the moderate event in early July 1982 (Fig. 8c) may be associated with a mesoscale eddy feature over the shelf evident in an infrared satellite image (Lentz 1987).

Explicit estimates of the vertical structure of the cross-shelf velocity depend on knowing the alongshelf pressure gradient. However, the cross-shelf velocity profiles are qualitatively consistent with relative magnitudes of the cross-shelf momentum flux divergence in the sense that the onshore return flow is in the interior for the Peru and Oregon shelves, where S and the cross-shelf momentum flux divergence are large, and the onshore return flow is in the bottom boundary layer for the northwest Africa shelf, where S and the cross-shelf momentum flux divergence are small. These observations indicate that the nonlinear cross-shelf momentum

TABLE 2. Estimates for each mooring site of the ratio of the mean divergence in cross-shelf momentum flux to the mean wind stress, the ratio of the standard deviation of the divergence in cross-shelf momentum flux to the standard deviation of the wind stress, and the regression slope and correlation between the subtidal divergence in the cross-shelf momentum flux and the wind stress.

Site	Time period (UTC)	S	Ratio			
			Means	Std dev	Regression slope	Correlation
Peru PSS	0000 5 Mar–0500 14 May 1977	1.50	0.72	1.36	0.62	0.46
Peru PS	0000 5 Mar–0500 14 May 1977	1.20	0.48	0.66	0.51	0.78
Oregon	0000 5 Jul–1900 28 Aug 1973	0.95	0.50	0.43	0.33	0.75
NC 1982	0000 15 Apr–1100 28 Jul 1982	0.48	0.30	0.40	0.14	0.35
NC 1981	0700 9 Apr–0500 13 Jul 1981	0.38	0.23	0.36	(0.056)	0.16*
NW Africa	1900 24 Feb–1100 26 Apr 1974	0.19	0.007	0.03	(0.003)	0.08*

* Correlations are not significantly different from zero at the 95% confidence level. The corresponding regression slopes are uncertain but small.

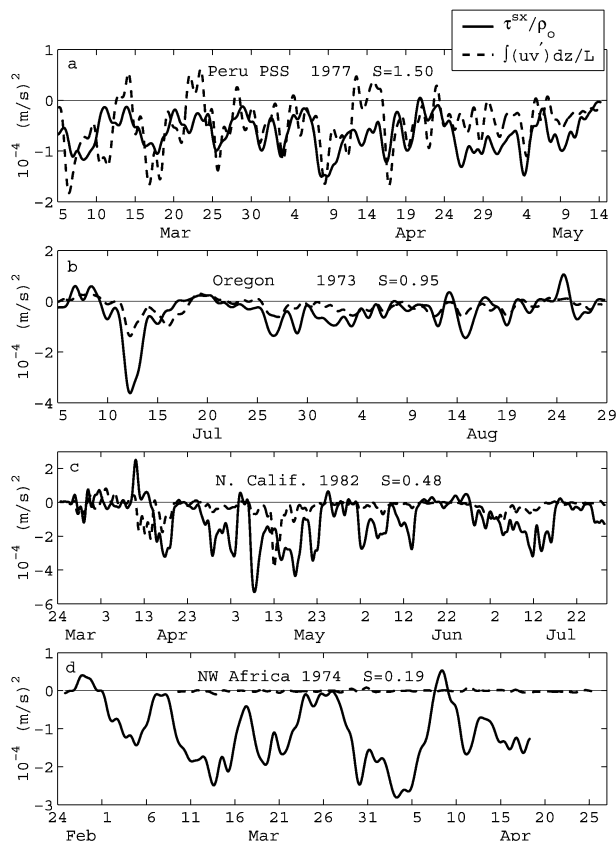


FIG. 8. Time series of τ^{sx}/ρ_o and $\int (uv') dz/L$ from (a) Peru (PSS site), (b) Oregon, (c) northern California, and (d) northwest Africa. Note that, where S is large, the magnitude of the cross-shelf momentum flux divergence is significant relative to the wind stress and is correlated with the wind stress. Where S is small, the cross-shelf momentum flux divergence is small and not correlated with the wind stress.

flux divergence is substantial relative to the wind stress at subtidal to monthly time scales in the coastal upwelling regions where the Burger number is 1–1.5 (Oregon and Peru).

b. Numerical model results

The theoretical development in section 2 and the comparison with observations in section 3a both focused primarily on the steady upwelling response. The time-dependent upwelling response is now examined using the Regional Ocean Model System (ROMS) in a two-dimensional configuration. This preliminary analysis using ROMS is not intended to be a thorough investigation of the time-dependent upwelling response [see Allen et al. (1995) and Austin and Lentz (2002) for more complete investigations of the time-dependent upwelling response]. Instead, the primary objectives of this analysis are 1) to determine the importance of the cross-shelf momentum flux divergence to the time-dependent response and its dependence on S , 2) to determine how

the vertical structure of the cross-shelf circulation varies with S , and 3) to identify some of the weaknesses and limitations of the theory presented in section 2.

ROMS is a free-surface, hydrostatic, primitive equation ocean model that uses stretched, terrain-following coordinates in the vertical and orthogonal curvilinear coordinates in the horizontal (see the ROMS Web site online at <http://marine.rutgers.edu/po/index.php?model=roms>, for details). The model is here configured in two dimensions (cross-shelf and vertical), in a periodic channel with length 2 km, using four alongshelf grid points with no alongshelf variations. The topography is given by $h = h_0 + \alpha y$, where $h_0 = 10$ m is the depth at the coast and $\alpha = 0.004$. For $y > 47.5$ km, the bottom is flat with $h = 200$ m. An offshore wall is located 160 km from the coast and does not affect the results presented here. Horizontal grid spacing is 1 km, while 30 vertical grid points are used with more grid points concentrated near the surface and bottom to resolve the boundary layers. Increased horizontal resolution does not substantially change the present results. Standard dynamical assumptions are made: no flow or density flux through solid boundaries, linearized bottom stress with a coefficient of $r = 5 \times 10^{-4} \text{ m s}^{-1}$, Mellor–Yamada level-2.5 turbulence closure scheme, uniform rotation with $f = 10^{-4} \text{ s}^{-1}$, and no explicit lateral mixing or viscosity. The ocean is initially at rest with a constant buoyancy frequency N . A constant, spatially uniform upwelling-favorable alongshelf wind stress ($\tau^{sx} = -0.1 \text{ Pa}$) is applied over the entire domain. The baroclinic time step is between 108 and 288 s, being smaller for larger N , while the barotropic time step is about 10 s.

Twelve model runs were made varying N from 0 to $5 \times 10^{-2} \text{ s}^{-1}$ so that S ranged from 0 to 2.0. As in previous numerical modeling studies (e.g., Allen et al. 1995; Austin and Lentz 2002), the upwelling response is unsteady and there are three regions to the flow, an inner-shelf region where the surface and bottom boundary layers merge ($y < 10$ km for $S = 1$, middle panel of Fig. 9), a middle region where interior isopycnals slope upward and there is a geostrophic alongshelf jet ($10 < y < 35$ km), and an offshore region where interior isopycnals are essentially level ($y > 35$ km). The focus here is on the middle region of upward sloping isopycnals where the mechanism described in section 2 may contribute to the cross-shelf momentum flux divergence. In this region the isopycnal slopes are approximately $0.25f/N$, similar to the observed mean isopycnal slopes (Fig. 3). The response is unsteady since the region of sloping isopycnals and the associated upwelling jet move offshore with time. This complicates interpretation of the numerical model results and precludes quantitative comparisons between the time-dependent numerical model results and the steady theory.

The structure of the cross-shelf velocity after 13 days varies substantially for different values of S (Fig. 9). For $S \leq 0.5$ the onshore return flow is concentrated in the bottom boundary layer. However, for $S \approx 1$, the

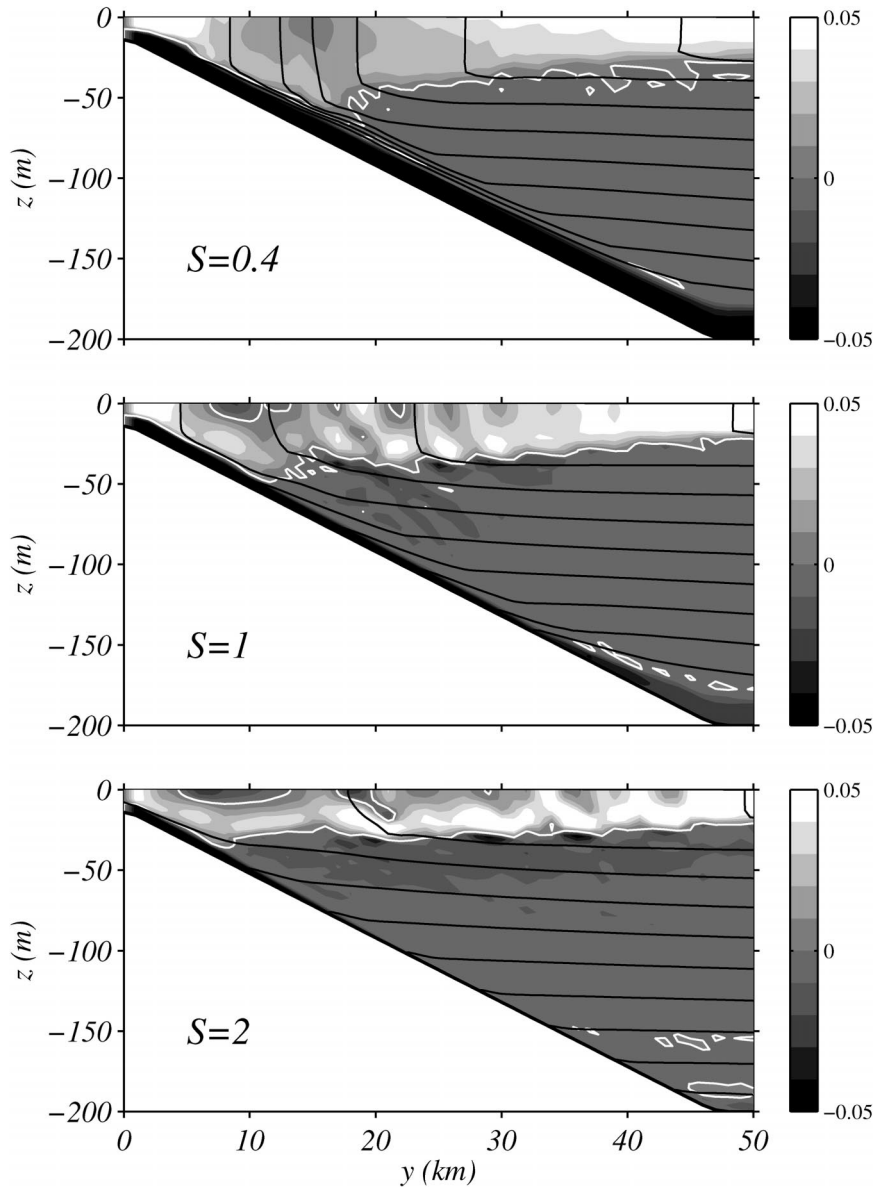


FIG. 9. The cross-shelf velocity as a function of depth and offshore distance after 13 days of a 0.1-Pa upwelling-favorable wind stress, from three numerical model runs with different Burger numbers (S). The grayscale for the cross-shelf velocities (m s^{-1}) is shown on the right and the white contours denote zero velocity. Isopycnals are shown by the black lines. Note that the onshore return flow (negative velocities) for $S = 0.4$ is largest in the bottom boundary layer, while for $S = 2.0$ it is largest just below the surface boundary layer.

onshore return flow ($10 < y < 35$ km) is spread more uniformly throughout the water column. As S approaches 2, the onshore return flow ($10 < y < 45$ km) is largest just below the surface boundary layer and there is essentially no return flow in the bottom boundary layer. The vertical structure of the cross-shelf flow for $S = 1$ is qualitatively consistent with the vertical structure of the mean cross-shelf flow over the Oregon and Peru shelves seen in Fig. 1. The dependence on S of the vertical structure of the onshore flow is consistent with

the steady theoretical prediction that the onshore return flow would be concentrated in the bottom boundary layer for small S and in the interior when S is one or larger. However, the numerical model results also emphasize a limitation of the theory; the assumption that the interior cross-shelf flow is vertically uniform.

To quantify the dependence on S , the cross-shelf transports in the surface and bottom boundary layers and in the interior were calculated for each numerical model run after 13 days at a position $y = 20$ km (see

Fig. 9). This location was chosen as representative of the region where interior isopycnals slope upward toward the coast. The surface boundary layer transport is estimated as transport above the uppermost zero crossing of the cross-shelf velocity. The bottom boundary layer transport is estimated as the transport below the top of the bottom boundary layer, which is approximated by the near-bottom depth at which there is a large change in the vertical shear of the cross-shelf velocity. The interior cross-shelf transport is estimated as the transport between the base of the surface boundary layer and the top of the bottom boundary layer because it is difficult to identify the portion of the interior transport that extends into the boundary layers. Consequently, this underestimates the interior transport as defined in (5) by the amount contained in the boundary layers. The surface boundary layer transport is approximately constant and equal to the wind-driven Ekman transport (not shown). The bottom boundary layer transport (normalized by the surface boundary layer transport) decreases with increasing S , while the normalized interior transport increases with increasing S (Fig. 5 symbols). These tendencies in the time-dependent numerical model results are consistent with the steady theory.

Estimation of the terms in the alongshelf momentum balance (2) reveals some discrepancies between the time-dependent numerical model results and the steady theory. The individual terms are estimated as average values from day 12 to day 14 over the region between $y = 10$ km and $y = 20$ km. Estimates of the cross-shelf momentum flux divergence are not very sensitive to the region chosen because the cross-shelf momentum flux exhibits an approximately linear increase from the coast to a maximum near the center of the upwelling jet. The bottom stress (normalized by the wind stress) decreases from about 1 for $S = 0$ to 0.4 for $S = 2$ (Fig. 4a symbols), consistent with the dependence of the bottom boundary layer transport on S (Fig. 5). The decrease is also qualitatively consistent with the steady theory, though the rate of decrease with increasing S is smaller than predicted by the steady theory assuming the proportionality constant $b = 1$. These results are also consistent with the numerical model results of Allen et al. (1995), who noted that the bottom stress did not balance the surface stress after 16 days, in three different runs. Their estimates of τ^{bx}/τ^{sx} (the average over the cross-shelf region from 50–150 km in their Fig. 15) exhibit a similar decrease with increasing Burger number (Fig. 4a). The stratification (N) in the model runs of Allen et al. (1995) is not constant with depth, which may account for the differences between the two sets of numerical runs. The Burger numbers for the model runs of Allen et al. were estimated using one-half of the maximum buoyancy frequency.

The cross-shelf momentum flux divergence (normalized by the wind stress) increases from 0 to 0.3 as S increases from 0 to 0.6 and is relatively constant for S between 0.6 and 2 (Fig. 4b symbols). The cross-shelf

momentum flux divergence does not continue to increase as S increases and hence is much smaller than predicted by the steady theory with $b = 1$. This discrepancy is largely due to a nonzero temporal acceleration term (Fig. 4c). That is, the numerical model has not reached steady state after 13 days in the region where the momentum terms are estimated. Consequently both the divergence in the cross-shelf momentum flux and the temporal acceleration contribute to the interior onshore transport seen in Fig. 5. This relationship between the momentum terms and the interior transport can be seen by dividing (2) by f and noting that the right-hand side (without the alongshelf pressure gradient) is equal to the interior cross-shelf transport ($v^i h$) from (5). Based on these numerical model calculations it is unclear whether a steady balance is ever reached in the region of upward sloping isopycnals and, if so, how the steady balance is achieved.

4. Discussion

a. Time scale to reach steady state

The simple theory presented in section 2 neglects temporal acceleration, which the numerical model results suggest can be important, even on time scales of 13 days or longer. In the context of the theory, an estimate of the time scale to reach steady state can be made by substituting the expression for the divergence of the cross-shelf momentum flux given in (10) into the alongshelf momentum balance (2) and then approximating the bottom stress with a linear drag law of the form $\tau^{bx} = \rho_o r u^b$. From (3) and (9), $u(z) \approx u^b - N(z + h)$ for upwelling. Substituting this expression into the acceleration term in (2) and calculating the vertical integral yields a first-order differential equation for u^b . The associated frictional adjustment time scale is

$$T_f = \frac{h}{r} \frac{1}{(1 + S/2)}.$$

This is only a slight reduction of the traditional frictional adjustment time scale h/r for larger values of S , in contrast to the numerical model results that suggest a longer adjustment time (Fig. 4). However, the theory does not consider either the adjustment of the interior density field or buoyancy advection in the bottom boundary layer (e.g., Chapman 2002). Both of these processes are likely to play a critical role in the overall adjustment. For example, buoyancy advection in the bottom boundary layer is evident in the numerical model calculations (near-bottom isopycnal tilts in Fig. 9) and may contribute to the persistence of the temporal acceleration term by reducing the bottom stress. In a more general sense, the theory presented in section 2 is incomplete because it does not account for the interplay between the adjustment of the density field and the cross-shelf circulation. This interplay is presently under investigation using the numerical model.

b. Downwelling

The theory presented in section 2 was derived for upwelling-favorable winds, but it can also be applied to downwelling by reversing the sign of the alongshelf wind stress and the isopycnal slopes. For downwelling winds ($\tau^{sx} > 0$) and no alongshelf pressure gradient, (11) and (12) are the same as for upwelling, except that the sign in front of each factor of $bS/2$ is reversed. Thus, in the downwelling case for $S < 2$, there is an onshore momentum flux that acts in the same direction as the wind stress, in contrast to upwelling. As a result, the bottom stress must be larger than the wind stress because it balances both the wind stress and the cross-shelf momentum flux divergence. At $S = 2$, for downwelling, (11) and (12) have a singularity, suggesting that a steady-state does not exist in the theory. For $S > 2$, there is a flow reversal near the bottom, and so the bottom stress acts in the same direction as the wind stress, and both are balanced by the cross-shelf momentum flux divergence. Two-dimensional numerical modeling studies (Allen and Newberger 1996) show that for downwelling the cross-shelf density gradients are concentrated in a narrow front, in contrast to upwelling (Allen et al. 1995). This suggests that there may not be a region of the flow where the theory is valid during downwelling because cross-shelf variations in $\partial\rho/\partial y$ cannot be neglected. However, Allen and Newberger (1996) do show that the bottom stress exceeds the wind stress by a factor of 3–7 within the front and that the magnitude of the bottom stress increases with S (their Fig. 13). This result is qualitatively consistent with the theoretical prediction that the bottom stress should exceed the wind stress, suggesting that the cross-shelf momentum flux divergence may be important.

5. Summary

A new theory is proposed for two-dimensional upwelling that relates the structure of the wind-driven cross-shelf circulation and associated dynamics in the region of upward sloping isopycnals to the stratification, the bathymetry, and the wind forcing. The theory provides estimates of the divergence of the nonlinear cross-shelf momentum flux and insight into its influence on both the dynamics and the cross-shelf circulation. The basic assumption is that the cross-shelf momentum flux is primarily due to the wind-driven cross-shelf circulation acting on the vertically sheared, geostrophic alongshelf flow, in a manner analogous to the offshore flux of heat during coastal upwelling. Thus, for example, during upwelling, there is a near-surface offshore flux of faster alongshelf flow and a deeper onshore flux of slower alongshelf flow. This is not a complete theory of two-dimensional coastal upwelling because it does not include the evolution of the density field in response to the circulation. Instead, the isopycnal slope is assumed to be proportional to f/N based on the assumption

that the cross-shelf scale of the sloping isopycnals is the baroclinic deformation radius (Charney 1955). This assumption is supported by the observed mean isopycnal slopes. The theory predicts that the importance of the cross-shelf momentum flux divergence relative to the wind stress depends on the strength of the stratification, as measured by the Burger number $S = \alpha N/f$, where α is the bottom slope, N is the buoyancy frequency, and f is the Coriolis parameter. For small Burger number (weak stratification), the cross-shelf momentum flux is small, the bottom stress balances the wind stress, and the onshore return flow is primarily in the bottom boundary layer. For Burger number of order 1 or greater (strong stratification), the cross-shelf momentum flux divergence is relatively large and primarily balances the wind stress. Consequently, the bottom stress is small, and most of the onshore return flow is in the interior.

Direct estimates of the cross-shelf momentum flux divergence were made using moored current observations from four coastal upwelling regions (northwest Africa, northern California, Oregon, and Peru). Although many characteristics of these coastal upwelling regions are similar (e.g., Lentz 1992), they span a wide range of Burger numbers (0.2–1.5). Both the mean and subtidal cross-shelf momentum flux divergence are substantial relative to the wind stress (50% or more) off Peru and Oregon, but are small off northwest Africa. The magnitude of the divergence in the nonlinear offshore momentum flux (normalized by the wind stress) scales with the Burger number (Fig. 7), supporting the new theory, specifically (13).

The cross-shelf momentum flux divergence is also found to increase with increasing S in the region of upward sloping isopycnals in time-dependent two-dimensional numerical model calculations of coastal upwelling. In the numerical model runs, the vertical position of the onshore return flow shifts from the bottom boundary layer for small S to the interior for $S \approx 1$ (Fig. 5), qualitatively consistent with the steady theory. However, the numerical model results and observed mean current profiles show that for $1 < S < 2$ the onshore return flow may be concentrated higher in the water column (Fig. 9) and thus is not vertically uniform as assumed in the steady theory. The temporal acceleration of the alongshelf flow is similar in magnitude to the divergence in the cross-shelf momentum flux after 13 days in the numerical model results, and both contribute to the interior onshore flow. At present it is unclear how long it takes to reach steady state or if a steady state is ever attained in the vicinity of the upwelling jet in the numerical model calculations.

An interesting feature of both the mean cross-shelf current profiles from several upwelling regions (Fig. 1) and the numerical model results is the concentration of the onshore return flow near the surface at larger Burger numbers. This suggests that the upwelling circulation, and particularly the depth from which water is upwelled, may be quite different in regions characterized by large

versus small Burger numbers. The dynamics that determine the vertical structure of the interior return flow, its dependence on S , and the relevance of this two-dimensional process to the vertical structure of the cross-shelf flow in the ocean (Fig. 1) is the subject of ongoing research.

Acknowledgments. Comments on an earlier version of this manuscript by Ken Brink, Rich Garvine, and John Trowbridge are greatly appreciated. We also appreciate the thorough reviews and constructive comments provided by two anonymous reviewers that helped improve this paper. This research was funded by the Ocean Sciences Division of the National Science Foundation under Grants OCE-9809965, OCE-0095059, and OCE-0241292.

REFERENCES

- Allen, J. S., 1980: Models of wind driven currents on the continental shelf. *Annu. Rev. Fluid Mech.*, **12**, 389–433.
- , and P. K. Kundu, 1978: On the momentum, vorticity and mass balance off the Oregon coast. *J. Phys. Oceanogr.*, **8**, 13–27.
- , and R. L. Smith, 1981: On the dynamics of wind-driven shelf currents. *Philos. Trans. Roy. Soc. London*, **A302**, 617–634.
- , and P. A. Newberger, 1996: Downwelling circulation on the Oregon continental shelf. Part I: Response to idealized forcing. *J. Phys. Oceanogr.*, **26**, 2011–2035.
- , P. A. Newberger, and J. Federiuk, 1995: Upwelling circulation on the Oregon continental shelf. Part I: Response to idealized forcing. *J. Phys. Oceanogr.*, **25**, 1843–1866.
- Austin, J. A., and S. J. Lentz, 2002: The inner shelf response to wind-driven upwelling and downwelling. *J. Phys. Oceanogr.*, **32**, 2171–2193.
- Badan-Dangon, A., 1998: Coastal circulation from the Galápagos to the Gulf of California. *The Sea*, A. R. Robinson and K. H. Brink, Eds., The Global Coastal Ocean Regional Studies and Syntheses, Vol. 11, John Wiley and Sons, 315–344.
- , K. H. Brink, and R. L. Smith, 1986: On the dynamical structure of the midshelf water column off northwest Africa. *Cont. Shelf Res.*, **5**, 629–644.
- Barber, R. T., and R. L. Smith, 1981: Coastal upwelling ecosystems. *Analysis of Marine Ecosystems*, A. R. Longhurst, Ed., Academic Press, 31–68.
- Barton, E. D., A. Huyer, and R. L. Smith, 1977: Temporal variation observed in the hydrographic regime near Cabo Corveiro in the northwest Africa upwelling region, February to April 1974. *Deep-Sea Res.*, **24**, 7–23.
- Brink, K. H., 1998: Deep-sea forcing and exchange processes. *The Sea*, K. H. Brink and A. R. Robinson, Eds., The Global Coastal Ocean Processes and Methods, Vol. 10, John Wiley and Sons, 151–167.
- , D. Halpern, and R. L. Smith, 1980: Circulation in the Peruvian upwelling system near 15°S. *J. Geophys. Res.*, **85**, 4036–4048.
- , B. H. Jones, J. C. V. Leer, C. N. K. Mooers, D. W. Stuart, M. R. Stevenson, R. C. Dugdale, and C. W. Heburn, 1981: Physical and biological structure and variability in an upwelling center off Peru near 15°S during March, 1977. *Coastal Upwelling*, F. A. Richards, Ed., Amer. Geophys. Union, 473–495.
- Brown, W. S., J. D. Irish, and C. D. Winant, 1987: A description of subtidal pressure field observations on the northern California shelf during the Coastal Ocean Dynamics Experiment. *J. Geophys. Res.*, **92**, 1605–1636.
- Bryden, H. L., D. Halpern, and R. D. Pillsbury, 1980: Importance of eddy heat flux in a heat budget for Oregon coastal waters. *J. Geophys. Res.*, **85**, 6649–6653.
- Chapman, D. C., 2002: Deceleration of a finite-width, stratified current over a sloping bottom: Frictional spindown or buoyancy shutdown? *J. Phys. Oceanogr.*, **32**, 336–352.
- Charney, J. G., 1955: The generation of oceanic currents by wind. *J. Mar. Res.*, **14**, 477–498.
- Dever, E. P., 1997: Wind-forced cross-shelf circulation on the northern California shelf. *J. Phys. Oceanogr.*, **27**, 1566–1580.
- , and S. J. Lentz, 1994: Heat and salt balances over the northern California shelf in winter and spring. *J. Geophys. Res.*, **99**, 16 001–16 017.
- Ekman, V. W., 1905: On the influence of the earth's rotation on ocean currents. *Arkiv. Math. Astron. Fys.*, **2**, 1–53.
- Federiuk, J., and J. S. Allen, 1995: Upwelling circulation on the Oregon continental shelf. Part II: Simulations and comparisons with observations. *J. Phys. Oceanogr.*, **25**, 1867–1889.
- Garvine, R. W., 1971: A simple model of coastal upwelling dynamics. *J. Phys. Oceanogr.*, **1**, 169–179.
- Hickey, B. M., 1984: The fluctuating longshore pressure gradient on the Pacific Northwest shelf: A dynamical analysis. *J. Phys. Oceanogr.*, **14**, 276–293.
- , 1998: Coastal oceanography of western North America from the tip of Baja California to Vancouver Island (8, E). *The Sea*, A. R. Robinson and K. H. Brink, Eds., The Global Coastal Ocean Regional Studies and Syntheses, Vol. 11, John Wiley and Sons, 345–394.
- Huyer, A., 1984: Hydrographic observations along the CODE Central Line off northern California, 1981. *J. Phys. Oceanogr.*, **14**, 1647–1658.
- , 1990: Shelf circulation. *The Sea*, B. L. Méhauté and D.M. Hanes, Eds., Ocean Engineering Science, Part B, Vol. 9, Wiley, 423–466.
- , and R. L. Smith, 1985: The signature of El Niño off Oregon, 1982–83. *J. Geophys. Res.*, **90**, 7133–7142.
- , and P. M. Kosro, 1987: Mesoscale surveys over the shelf and slope in the upwelling region near Point Arena, California. *J. Geophys. Res.*, **92**, 1655–1681.
- , E. J. C. Sobey, and R. L. Smith, 1979: The spring transition in currents over the Oregon continental shelf. *J. Geophys. Res.*, **84**, 6995–7011.
- Large, W. G., and S. Pond, 1981: Open ocean momentum flux measurements in moderate to strong winds. *J. Phys. Oceanogr.*, **11**, 324–336.
- Lee, T. N., W. J. Ho, V. Kourafalou, and J. D. Wang, 1984: Circulation on the continental shelf of the southeastern United States. Part I: Subtidal response to wind and Gulf Stream forcing during winter. *J. Phys. Oceanogr.*, **14**, 1001–1012.
- , E. J. Williams, R. E. Wang, and L. Atkinson, 1989: Response of South Carolina continental shelf waters to wind and Gulf Stream forcing during winter of 1986. *J. Geophys. Res.*, **94**, 10 715–10 754.
- Lentz, S. J., 1987: A heat budget for the northern California shelf during CODE 2. *J. Geophys. Res.*, **92**, 14 491–14 509.
- , 1992: The surface boundary layer in coastal upwelling regions. *J. Phys. Oceanogr.*, **22**, 1517–1539.
- , 1994: Current dynamics over the northern California inner shelf. *J. Phys. Oceanogr.*, **24**, 2461–2478.
- , 1995: U.S. contributions to the physical oceanography of continental shelves in the early 1990's. *Rev. Geophys.*, **33** (Suppl.), 1225–1236.
- , and C. D. Winant, 1986: Subinertial currents on the southern California shelf. *J. Phys. Oceanogr.*, **16**, 1737–1750.
- , and J. H. Trowbridge, 1991: The bottom boundary layer over the northern California shelf. *J. Phys. Oceanogr.*, **21**, 1186–1201.
- , and —, 2001: A dynamical description of fall and winter mean current profiles over the northern California shelf. *J. Phys. Oceanogr.*, **31**, 914–931.
- , R. T. Guza, S. Elgar, F. Feddersen, and T. H. C. Herbers, 1999: Momentum balances on the North Carolina inner shelf. *J. Geophys. Res.*, **104**, 18 205–18 226.

- Pedlosky, J., 1978: An inertial model of steady coastal upwelling dynamics. *J. Phys. Oceanogr.*, **8**, 171–177.
- Richman, J. G., and A. Badan-Dangon, 1983: Mean heat and momentum budgets during upwelling for the coastal waters off northwest Africa. *J. Geophys. Res.*, **88**, 2626–2632.
- Scott, J. T., and G. T. Csanady, 1976: Nearshore currents off Long Island. *J. Geophys. Res.*, **81**, 5401–5409.
- Shillington, F. A., 1998: The Benguela upwelling system off southwestern Africa (16, E). *The Sea*, A. R. Robinson and K. H. Brink, Eds., The Global Coastal Ocean Regional Studies and Syntheses, Vol. 11, John Wiley and Sons, 583–604.
- Smith, R. L., 1981: A comparison of the structure and variability of the flow field in three coastal upwelling regions: Oregon, Northwest Africa, and Peru. *Coastal Upwelling*, F. A. Richards, Ed., Amer. Geophys. Union, 107–118.
- , 1995: The physical processes of coastal ocean upwelling systems. *Upwelling in the Ocean: Modern Processes and Ancient Records*, C. P. Summerhayes et al., Eds., John Wiley and Sons, 39–64.
- Strub, P. T., J. M. Mesías, V. Montecino, J. Rutllant, and S. Salinas, 1998: Coastal ocean circulation off western South America (6, E). *The Sea*, A. R. Robinson and K. H. Brink, Eds., The Global Coastal Ocean Regional Studies and Syntheses, Vol. 11, John Wiley and Sons, 273–314.
- Sverdrup, H. U., 1938: On the process of upwelling. *J. Mar. Res.*, **1**, 155–164.
- Trowbridge, J. H., and S. J. Lentz, 1998: Dynamics of the bottom boundary layer on the northern California shelf. *J. Phys. Oceanogr.*, **28**, 2075–2093.
- Winant, C. D., 1980: Coastal circulation and wind induced currents. *Annu. Rev. Fluid Mech.*, **12**, 271–301.
- , R. Beardsley, and R. Davis, 1987: Moored wind, temperature and current observations made during CODE-1 and CODE-2 over the northern California continental shelf and upper slope. *J. Geophys. Res.*, **92**, 1569–1604.
- Zamudio, L., and M. López, 1994: On the effect of the alongshore pressure gradient on numerical simulations over the northern California continental shelf. *J. Geophys. Res.*, **99**, 16 117–16 129.